THE JOURNAL OF PHYSICAL CHEMISTRY C

Article

pubs.acs.org/JPCC

$Li_{4+x}(Si_{1-x}Al_x)O_4$ Solid Solution Mechanosynthesis and Kinetic Analysis of the CO_2 Chemisorption Process

José Ortiz-Landeros,[†] Issis C. Romero-Ibarra,[‡] Carlos Gómez-Yáñez,[†] Enrique Lima,[‡] and Heriberto Pfeiffer*[,‡]

[†]Departamento de Ingeniería Metalúrgica, Escuela Superior de Ingeniería Química e Industrias Extractivas, IPN, UPALM, Av. Instituto Politécnico Nacional s/n, CP 07738, México DF, Mexico

[‡]Instituto de Investigaciones en Materiales, Universidad Nacional Autónoma de México, Circuito exterior s/n, Ciudad Universitaria, Del. Coyoacán, CP 04510, México DF, Mexico

ABSTRACT: Different Al-containing Li_4SiO_4 samples ($Li_{4+x}(Si_{1-x}Al_x)O_4$ solid solutions) were obtained by mechanosynthesis and then characterized structurally (X-ray diffraction (XRD) and solid-state NMR) and microstructurally (N_2 adsorption and scanning electron microscopy (SEM)). While solid-state NMR results showed that the aluminum (silicon) presented some distortion after the milling process, the milling process tended to increase the $Li_{4+x}(Si_{1-x}Al_x)O_4$ surface areas. The samples were tested dynamically and isothermally in the CO_2 chemisorption at high temperatures. In the second case, a complete kinetic analysis was produced. It was evidenced that aluminum addition and the new microstructural features produced during the milling process importantly increase the CO_2 capture, in comparison to the Li_4SiO_4 phase and the $Li_{4+x}(Si_{1-x}Al_x)O_4$ solid solutions prepared by solid-state reaction.

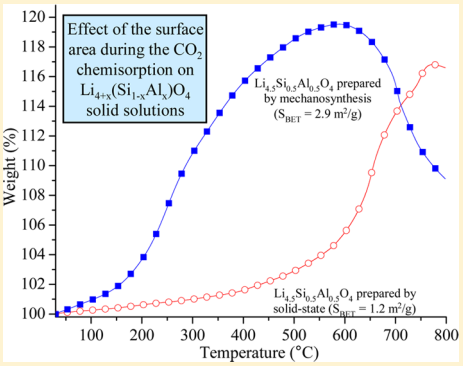

INTRODUCTION

One of the most threatening problems concerning atmospheric pollution is the anthropogenic carbon dioxide (CO_2) emissions.[1] An alternative solution to diminish the magnitude of these emissions is focused on the CO_2 capture or sequestration from flue gases by using solid sorbents.[2−5] Among these possible CO_2 captors, alkaline ceramics such as Li_2ZrO_3, Li_4SiO_4, Li_2CuO_2, Li_5AlO_4, Li_2SiO_3, Na_2ZrO_3, $Li_6Zr_2O_7$, and Li_8SiO_6 have shown excellent CO_2 capture properties.[4,6−34] These materials are able to chemisorb CO_2 in a wide temperature range and partial pressures. However, these materials present two limitations related to their relatively low reaction rates and kinetics.[6s,16,23,28−31]

In a recent study, different $Li_{4+x}(Si_{1-x}Al_x)O_4$ solid solutions were proposed as potential CO_2 sorbents.[31] These solid solutions were designed to enhance lithium ion diffusion in Li_4SiO_4-based materials in such a way that the CO_2 chemisorption process is promoted. The selection of an Al^{3+} metal ion as dopant was based on basic structural considerations, the defect chemistry of the system, and other thermodynamic considerations previously proposed for the design of fast ionic conductors.[35,36] It was corroborated that Al^{3+} ions occupy the Si^{4+} sites in the Li_4SiO_4 crystal lattice, leading to the generation of lithium interstitials. The corresponding defect formation reaction (eq 1) manifests a charge compensation mechanism as follows

$$Li_5AlO_4 \xrightarrow{Li_4SiO_4} 8Li_{Li} + Si_{Si} + Al'_{Si} + Li_i^{\bullet} + 8O_O \qquad (1)$$

Additionally, it was observed that the incorporation of aluminum into the Li_4SiO_4 structure highly improves the CO_2 capture properties at $T \geq 650$ °C. Also, when this alkaline ceramic reacts with CO_2, some secondary phases containing lithium are formed, and it has been shown that the diffusion properties of lithium in such secondary phases contribute to the CO_2 chemisorption.[11]

However, these solid solutions have been synthesized via the conventional route of solid-state reaction, like most of the alkaline ceramics reported so far as potential CO_2 captors. Actually, only a few alternative processing routes have been explored. In this context, a high-energy milling technique constitutes an attractive option for the preparation of compositionally homogeneous and fine ground powders with enhanced reactivity.[37−39] High-energy milling and related synthesis routes, such as mechanical alloying, mechanical activation, and mechanochemical synthesis (mechanosynthesis), have been able to produce ceramic solid solutions and compounds with complex compositions and refined microstructures. In fact, the reactivity of solids is strongly influenced by mechanochemical treatment. Hence, the milling process is widely used in the chemical industry where solids are involved. In addition, the preparation and activation of Li_4SiO_4 via shaking milling was recently published. This material showed an enhanced reactivity and therefore improved CO_2

Received: January 21, 2013
Revised: March 4, 2013
Published: March 4, 2013

   dx.doi.org/10.1021/jp4006982 | J. Phys. Chem. C 2013, 117, 6303−6311

capture properties compared to the sorbent prepared by solid-state reaction.[39]

Therefore, the aim of the present study was to analyze both structural and microstructural characteristics of $Li_{4+x}(Si_{1-x}Al_x)O_4$ solid solutions prepared via mechanosynthesis and its importance on the CO_2 chemisorption properties. The formation of the aluminum-containing solid solutions via this method is expected to enhance the performance of the obtained ceramic sorbents due to an increment of the lithium diffusion produced by the interstitial atoms, a high surface area, and a high compositional homogeneity in the material.

EXPERIMENTAL SECTION

$Li_{4+x}(Si_{1-x}Al_x)O_4$ solid solutions, varying the aluminum content in the range $0.1 \leq x \leq 0.5$, were synthesized by the mechanochemical technique starting from stoichiometric amounts of Li_4SiO_4 and Li_5AlO_4 ceramic binary oxides. These two ceramics were prepared by solid-state reaction as it had been previously described.[31] The mechanosynthesis was performed into a high energy shaker mill (Model Spex Sample-Prep 8000M) equipped with a cylindrical zirconia vial and zirconia balls as milling media. Samples were prepared using a balls:powder mixture weight ratio of 30:1 and different milling times of 30, 45, 60, and 90 min. Samples were labeled according to the amount of aluminum added. For example, the 20m corresponds to the $Li_{4.2}(Si_{0.8}Al_{0.2})O_4$, i.e., a nominal composition of $x = 0.2$. Additionally, pure Li_4SiO_4 prepared by conventional solid-state reaction was used for comparison purposes; this sample was simply labeled as Li_4SiO_4.

The samples were characterized by different techniques such as powder X-ray diffraction (XRD), solid-state nuclear magnetic resonance (NMR), N_2 adsorption, scanning electron microscopy (SEM), and thermogravimetric analysis (TGA). The XRD patterns were obtained with a BRUKER axs Advance D8 diffractometer coupled to a Cu anode X-ray tube. The $k_{\alpha 1}$ wavelength was selected with a diffracted beam monochromator, and the compounds were identified conventionally using the PDF database. NMR spectra were acquired on a Bruker Avance II spectrometer with a magnetic field strength of 7.05 T, corresponding to a ^{27}Al Larmor frequency of 78.3 MHz. Short single pulses ($\pi/12$) with a recycle time of 0.5 s were used. Samples were packed into zirconia rotors with 4 mm o.d. The ^{27}Al chemical shift was expressed as parts per million from an aqueous solution of $Al(NO_3)_3$ as the external standard. ^{29}Si MAS NMR spectra were obtained operating the spectrometer at a resonance frequency of 59.59 MHz with a recycling time of 40 s and a pulse time of 3 μs. The spinning frequency was 5 kHz, and tetramethylsilane (TMS) was used as a reference. Surface area analyses were performed in Minisorp II equipment from BEL-Japan. The N_2 adsorption isotherms were determined at 77 K by volumetric adsorption. Before the N_2 adsorption process, all the samples were outgassed at room temperature for 24 h. Surface areas were calculated with the BET equation. The morphology of the samples was analyzed by SEM, using a JEOL JMS-7600F microscope. Different thermal analyses were performed in Hi-Res TGA Q500HR thermogravimetric equipment from TA Instruments. A set of samples was heat-treated, with a heating rate of 5 °C/min, from room temperature to 800 °C. The analyses were carried out in a CO_2 atmosphere (Praxair, grade 3.0). Additionally, other samples were analyzed isothermally between 350 and 600 °C for 4 h.

RESULTS AND DISCUSSION

All the $Li_{4+x}(Si_{1-x}Al_x)O_4$ solid solutions, i.e., $0.1 \leq x \leq 0.5$, were successfully synthesized via high energy ball milling. Figure 1 shows the XRD patterns of the 10m samples prepared

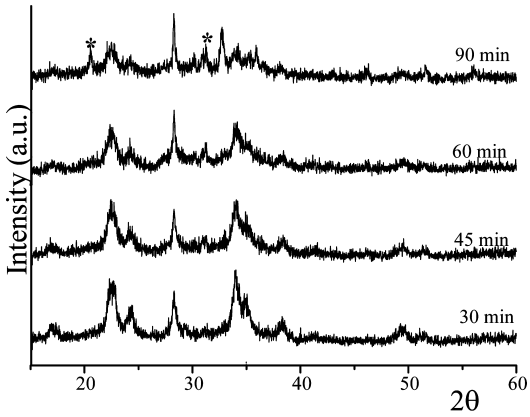

Figure 1. XRD patterns of the 10m sample prepared during different milling times. * contamination coming from the milling media.

at different times (30, 45, 60, and 90 min). XRD results suggested that using high energy milling it is possible to dissolve the Li_5AlO_4 phase into the Li_4SiO_4 lattice, based on previous studies; it is assumed that the Al^{3+} ion occupies the Si^{4+} ion sites in the orthosilicate structure.[31] Actually, this fact was later probed by NMR. Additionally, from these XRD patterns it is evident that samples presented small crystal sizes, as the diffraction peaks are considerably wide. Then, the mechanosynthesis method seems to be a good alternative for synthesizing homogeneous Li_4SiO_4-based solid solutions without further calcination steps. It must be noticed that despite all the samples presented similar behavior to form a complete solid solution longer milling times than 60 min promoted the sample contamination with material coming from the milling media. At 90 min, the zirconium oxide was identified in Figure 1. For the sake of brevity, and to avoid the presence of an undesirable secondary phase, only the solid solutions prepared by milling during 60 min were further studied.

To complement the XRD analysis and to further analyze the ball-milled solid solutions, a solid-state NMR analysis was performed. Figure 2 shows the ^{27}Al MAS NMR spectra of three different $Li_{4+x}(Si_{1-x}Al_x)O_4$ solid solutions (10m, 30m, and

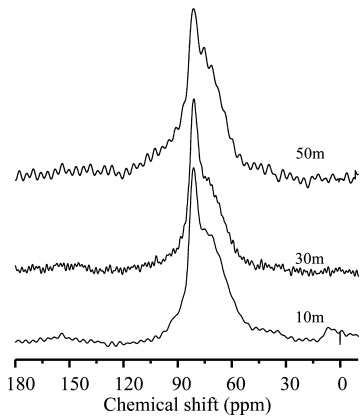

Figure 2. ^{27}Al MAS NMR spectra of different $Li_{4+x}(Si_{1-x}Al_x)O_4$ solid solutions.

dx.doi.org/10.1021/jp4006982 | J. Phys. Chem. C 2013, 117, 6303−6311

50m). The presence of a wide and asymmetric NMR signal can be seen, which suggests a spread of chemical shift of aluminums 4-fold coordinated. The main peak is located at 82 ppm, and the other convoluted peaks are located between 82 and 70 ppm. In a previous paper,[31] it was reported that similar $Li_{4+x}(Si_{1-x}Al_x)O_4$ solid solutions prepared by solid-state reaction presented two well-defined ^{27}Al 4-fold coordinated peaks at 82 and 68 ppm. Additionally, the peak located at 68 ppm increased as a function of the aluminum content. In the present case, the peak located at 82 ppm was always the more intense. Therefore, the aluminum sites presented an alteration of their chemical environment by the milling process, which may have some influence during the CO_2 chemical capture. Actually, the ^{29}Si MAS NMR spectra (Figure 3), independently

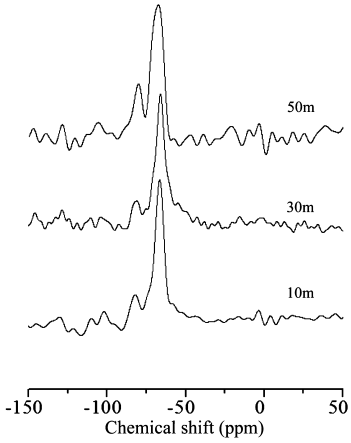

Figure 3. ^{29}Si MAS NMR spectra of different $Li_{4+x}(Si_{1-x}Al_x)O_4$ solid solutions.

of the aluminum content, were composed by two resonance lines at −67 and −82 ppm. The peak centered at −67 ppm corresponded to the $(SiO_4)^{4-}$ tetrahedral linked to four silicon atoms as currently occurs in a SiO_2 network. However, the second NMR peak observed at −82 ppm is assigned to the $(SiO_4)^{4-}$ tetrahedral connected to three silicon atoms and one aluminum atom which means that aluminum is incorporated into the silica framework. With an increase of the aluminum content, the intensity of the peak due to Si(1Al) units increases, but no additional peaks at stronger fields were observed, suggesting that aluminum is well distributed and that no enriched aluminum microdomains were formed. This result is relevant, as previously,[31] when $Li_{4+x}(Si_{1-x}Al_x)O_4$ solid solutions were prepared by solid-state reaction, it was concluded that aluminum ions did not migrate into the SiO_2 framework.

For the microstructural analysis, both N_2 adsorption−desorption and SEM experiments were performed. In the N_2 adsorption experiments all the samples presented isotherms type II (data not shown) according to the IUPAC,[40,41] which correspond to nonporous or macroporous materials. Table 1 shows the surface area values obtained by fitting N_2 isotherm data to the BET model.[40] In any case, all the samples prepared by milling presented higher surface areas than the Li_4SiO_4 sample prepared by solid-state reaction (0.4 m^2/g). Thus, the surface area values of solid solutions did not present significant changes as a function of the aluminum content, and the milling process seems to be mainly responsible for the final surface area.

Table 1. BET Surface Areas of the Different $Li_{4+x}(Si_{1-x}Al_x)O_4$ Solid Solutions Prepared by Mechanochemical Synthesis

sample	surface area, (S_{BET}, m^2/g)
Li_4SiO_4[a]	0.4
10m	2.4
30m	2.3
50m	2.9

[a]Sample prepared by a solid-state reaction.

Figure 4 shows the SEM images in different zones of the Li_4SiO_4 sample prepared by solid-state reaction and the $Li_{4.5}(Si_{0.5}Al_{0.5})O_4$ milled sample (50m). Samples 10m and 30m present features similar to the $Li_{4.5}(Si_{0.5}Al_{0.5})O_4$, independently of the aluminum content. The Li_4SiO_4 (Figure 4A) presented dense particles, with an average particle size of 40−60 μm. Similar results were reported.[39] The Li_4SiO_4 usually presents dense, non-corrugated, and large micrometric particles (>60 μm[39]) when it is prepared by solid-state reaction. In the present case, Li_4SiO_4 presented dense and slightly corrugated particles, with an average particle size of 40−60 μm. Conversely, the ball milling samples presented important morphological changes. The milling process produced $Li_{4+x}(Si_{1-x}Al_x)O_4$ agglomerates of 10−25 μm (inset of Figure 4B), which were composed of small particles (1−4 μm). Additionally, the particle surface showed the presence of some important roughness. From these images, it is clear that $Li_{4+x}(Si_{1-x}Al_x)O_4$ solid solutions have small particle size and a more complex surface roughness. These morphological features are consistent with the N_2 adsorption−desorption results previously presented.

The CO_2 chemisorption in the $Li_{4+x}(Si_{1-x}Al_x)O_4$ solid solutions has been described as follows

$$Li_{4+x}(Si_{1-x}Al_x)O_4 + (1+x)CO_2 \rightarrow (1+x)Li_2CO_3 + (1-x)Li_2SiO_3 + xLiAlO_2 \quad (2)$$

wherein the aluminum addition implies the presence of lithium excess, in comparison to the pure Li_4SiO_4 sample. In this sense, all the milled solid solutions showed significant CO_2 chemisorption improvement during the TGA analyses using a CO_2 atmosphere (Figure 5). First, Li_4SiO_4 presented the known and typical CO_2 chemisorption; Li_4SiO_4 increased its weight by about 4 wt %, which is in good agreement with previous reports, for a dynamic TG experiment.[6,11,30,31] The chemisorption process began at ∼460 °C, and the maximum chemisorption was obtained and stabilized at 585 °C. On the other hand, CO_2 chemisorption was importantly increased in the aluminum containing samples. The CO_2 chemisorption was produced between ∼50 and 585 °C in all milled samples, a remarkably larger temperature range than in the case of Li_4SiO_4.

It must be mentioned that in a previous work Li_4SiO_4 was mechanically activated, and its CO_2 chemisorption capacities increased significantly in comparison to the solid-state sample.[39] On the basis of the above, the $Li_{4+x}(Si_{1-x}Al_x)O_4$ solid solutions must present a similar behavior as a result of the milling process. Moreover, the CO_2 chemisorption increased as a function of the aluminum content from 8.7 to 19.6 wt % for the 10m and 50m samples, respectively. Therefore, the CO_2 chemisorption was increased by adding aluminum, although the samples did not present important differences in their surface

dx.doi.org/10.1021/jp4006982 | J. Phys. Chem. C 2013, 117, 6303−6311

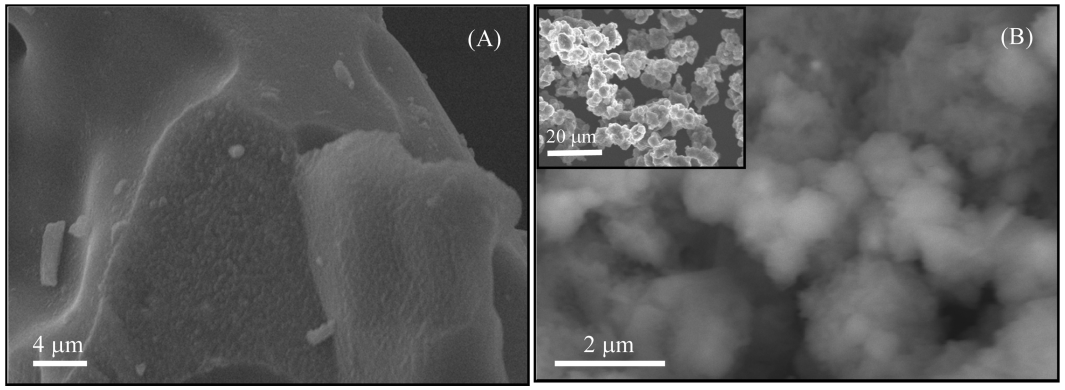

Figure 4. SEM images of the Li_4SiO_4 sample prepared by solid-state reaction (A) and 50m sample (B); the latter shows the morphological features obtained in the different $Li_{4+x}(Si_{1-x}Al_x)O_4$ solid solutions.

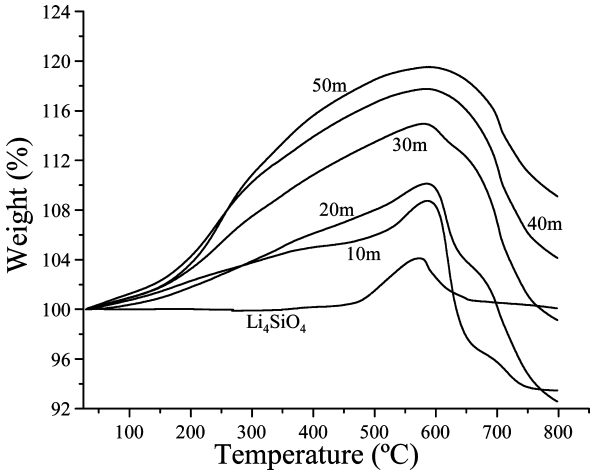

Figure 5. Thermogravimetric dynamic curves of different $Li_{4+x}(Si_{1-x}Al_x)O_4$ solid solutions in a flux of CO_2.

area. These results suggest that the CO_2 chemisorption improvements are related not only to the milling process but also mainly to the aluminum content. Finally, something else can be observed during the desorption process at temperatures higher than 650 °C (Figure 5); some samples lost more weight than that previously chemisorbed. The weight lost is attributed to a previous carbonation of the sample, which must be produced during the synthesis and handling of the sample, corroborating the higher reactivity of these materials.

In a previous paper[31] it was described that Al-doped Li_4SiO_4 samples synthesized by solid-state reaction chemisorbed CO_2 in a wider temperature range than Li_4SiO_4. In those samples the most important CO_2 chemisorption was produced at high temperatures, 600−770 °C. The variations observed by the aluminum addition on the CO_2 chemisorption processes were correlated to the different lithium secondary phases produced in each case and their corresponding lithium ion diffusion properties.

Table 2 shows the maximum weight increments observed in the aluminum containing solid solutions prepared via mechanosynthesis and conventional solid-state reaction techniques, for comparison purposes.[31] It can be noticed that samples prepared by mechanosynthesis exhibit a higher CO_2 capture at lower temperatures. Figure 6 shows the CO_2 chemisorption observed on the $Li_{4.5}(Si_{0.5}Al_{0.5})O_4$ samples prepared by solid-state reaction and mechanosynthesis (50m). From these curves

Table 2. Maximum CO_2 Chemisorption in the Different Materials

sample	maximum CO_2 chemisorption observed at temperatures <600 °C (wt %)	samples prepared via solid-state reaction[31]	maximum CO_2 chemisorption observed at temperatures between 600 and 770 °C (wt %)
10m	8.8	10SS	4.7
20m	10.1	20SS	8.4
30m	15.0	30SS	10.6
40m	17.9	40SS	11.1
50m	19.6	50SS	16.8

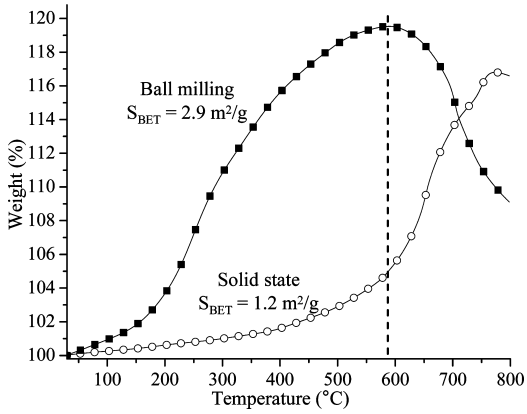

Figure 6. Comparison of the TG dynamic curves of the following samples: 50m and $Li_{4.5}Si_{0.5}Al_{0.5}O_4$ sample prepared by solid-state reaction,[31] in a flux of CO_2.

it is clear that the milled sample presented a higher CO_2 chemisorption at lower temperatures, although it was proved that the aluminum addition only improves the CO_2 chemisorption at T > 600 °C in the solid-state samples.[31] Additionally, it has to be mentioned that both samples presented different surface areas. Therefore, it is important to highlight the fact that CO_2 chemisorption produced in the milled samples highly depends on two different factors: (1) the $Li_{4+x}(Si_{1-x}Al_x)O_4$ solid solution composition and (2) the specific microstructural properties (surface area) obtained during the milling process.

To further analyze the CO_2 chemisorption behavior of the samples, a kinetic analysis was performed. As expected, all these experiments followed a typical behavior (Figure 7), wherein the CO_2 chemisorption increased as a function of temperature in

dx.doi.org/10.1021/jp4006982 | J. Phys. Chem. C 2013, 117, 6303−6311

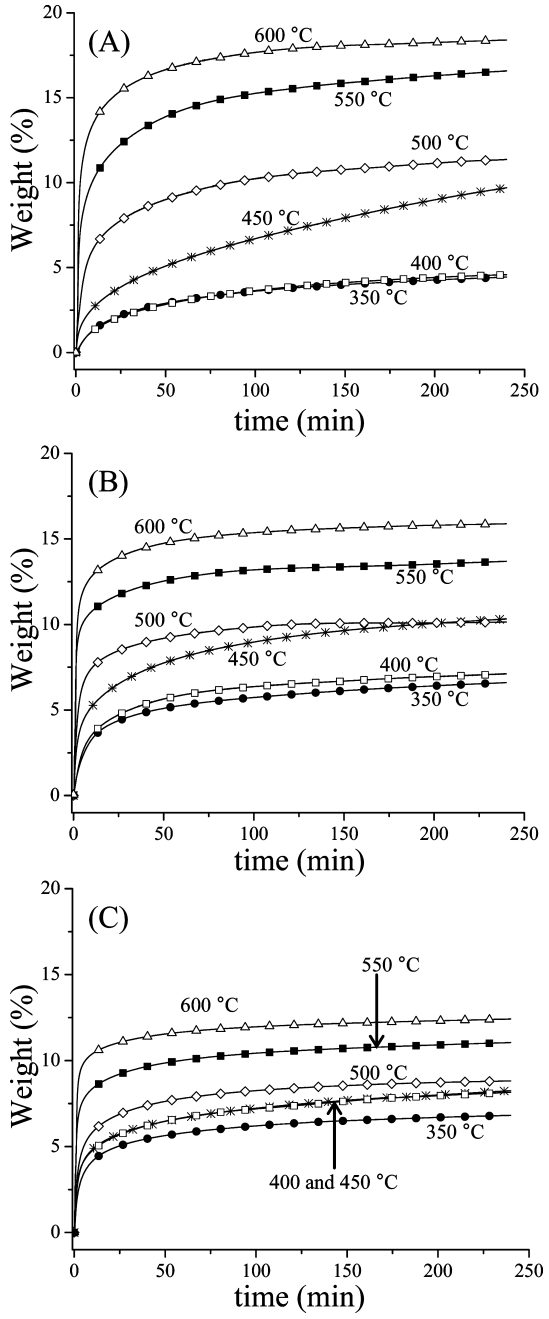

Figure 7. CO_2 capture analyses of different $Li_{4+x}(Si_{1-x}Al_x)O_4$ solid solutions with varying temperature (350−600 °C).

an exponential manner. For the 10m sample (Figure 7A), while the experiments performed at 350 and 400 °C chemisorbed only about 4.5 wt % of CO_2 after 4 h, the total weight increment observed at 600 °C was 17.9 wt % for the same period of time. It means that at 600 °C the 10m sample showed an important increment of the CO_2 chemisorption in comparison to lower temperatures, and it had a final efficiency of 46.7%. In previous works,[6,11,30] the CO_2 chemisorption curves obtained in Li_4SiO_4 samples, at the same temperature range, showed efficiencies equal to or lower than 35.5%. This result can be explained not only by the enhanced microstructural properties but also by the change in the surface chemistry of the sorbents as a result of the aluminum content, as it was probed by the ^{27}Al NMR experiments. In other words, $Li_{4+x}(Si_{1-x}Al_x)O_4$ solid solutions prepared via mechanosynthesis show surface areas significantly larger than those obtained in the previous papers. Additionally, the aluminum addition must have modified the lithium basic chemical character, favoring the CO_2 chemisorption.

However, when the aluminum content increased in the $Li_{4+x}(Si_{1-x}Al_x)O_4$ samples, the final CO_2 chemisorption decreased at $T \geq 450$ °C (Figures 7B and 7C). The maxima chemisorptions obtained, in all the cases at 600 °C, were 15.8 and 12.4 wt % for 30m and 50m samples, respectively. These results are in agreement with the following different factors: (1) Aluminum contents decrease the particle surface area, which must limit the CO_2 chemisorption through the diffusion processes and (2) the formation and presence of secondary phases, such as $LiAlO_2$, only increases the lithium ion diffusion at $T > 600$ °C;[11,31] at lower temperatures $LiAlO_2$ acts as a barrier.

Although different models have been proposed in the literature,[6,16,21,29,30,42−45] these experimental data were fitted to a double exponential model (eq 3),[6,16,30] assuming that there are two global processes taking place during the CO_2 capture on $Li_{4+x}(Si_{1-x}Al_x)O_4$ solid solutions: (1) The CO_2 chemisorption produced directly over the $Li_{4+x}(Si_{1-x}Al_x)O_4$ surface (k_1) and (2) the CO_2 chemisorption kinetically controlled by diffusion processes (k_2). The second process occurs once the carbonate-oxide external shell is totally formed. Then, the double exponential model proposed is

$$y = A\ \exp^{-k_1 t} + B\ \exp^{-k_2 t} + C \qquad (3)$$

where y represents the weight percentage of the CO_2 chemisorbed; t is the time; and k_1 and k_2 are the exponential constants for the CO_2 chemisorption produced directly over the particles and the CO_2 chemisorption kinetically controlled by diffusion processes, respectively. The pre-exponential factors A and B indicate the intervals at which each process controls the whole CO_2 capture process, and the C constant indicates the y-intercept.

Table 3 shows the constant values related to direct chemisorption (k_1) and chemisorption kinetically controlled by diffusion processes (k_2) including the pre-exponential constants and R^2 values. Initially, it can be seen that k_1 values are, at least, 1 order of magnitude higher than those obtained for the k_2 constants, independently of the aluminum content. Thus, the CO_2 chemisorption process controlled by diffusion processes is the limiting step of the whole reaction process independently of the sample. Additionally, it can be seen that although the aluminum addition tends to increase the magnitude of both kinetic constants the k_1 values presented higher increments than k_2. Actually, the diffusion processes do not seem to be modified by the aluminum addition, and it must be related to the $LiAlO_2$ presence, which only enhances the lithium diffusion at $T > 600$ °C.[11] Conversely, the CO_2 direct chemisorption seems to be more influenced by the aluminum content even though all the milled samples showed similar surface area values. Therefore, the aluminum content must modify the superficial chemical properties of the $Li_{4+x}(Si_{1-x}Al_x)O_4$ solid solutions. The aluminum must increase the number of lithium-basic on the $Li_{4+x}(Si_{1-x}Al_x)O_4$ surface, which could be claimed to be especially active sites during the CO_2 chemisorption process.

From Table 3, something else must be noticed. The A and B pre-exponential values do not follow a common trend. In all the cases, the A values are smaller than B values, at low

dx.doi.org/10.1021/jp4006982 | J. Phys. Chem. C 2013, 117, 6303−6311

Table 3. CO_2 Chemisorption Kinetic Parameters of the Different $Li_{4+x}(Si_{1-x}Al_x)O_4$ Solid Solutions Prepared by Mechanosynthesis

T (°C)	k_1 (s^{-1})	k_2 (s^{-1})	A	B	C	R^2
			10m			
350	0.0138	0.00016	−1.895	−2.993	4.913	0.9996
400	0.0017	0.00017	−1.518	−3.531	5.074	0.9998
450	0.00152	0.00007	−2.632	−11.269	14.735	0.9993
500	0.00365	0.00025	−6.672	−5.862	12.823	0.9986
550	0.00749	0.00032	−12.050	−8.241	19.584	0.9940
600	0.00963	0.00041	−17.954	−6.904	22.356	0.9920
			30m			
350	0.00219	0.00016	−3.972	−3.065	7.334	0.9988
400	0.00255	0.00025	−3.941	−3.472	7.638	0.9972
450	0.00474	0.00023	−4.267	−5.467	10.402	0.9972
500	0.00728	0.00041	−7.731	−3.590	11.264	0.9985
550	0.01525	0.00041	−13.784	−4.021	15.634	0.9929
600	0.01174	0.00039	−16.811	−4.299	18.686	0.9911
			50m			
350	0.00423	0.00024	−4.134	−2.775	7.3241	0.9962
400	0.00585	0.00022	−4.601	−3.824	8.928	0.9934
450	0.00533	0.0002	−4.715	−3.838	9.080	0.9956
500	0.00584	0.00032	−5.590	−3.454	9.910	0.9951
550	0.01313	0.00032	−9.775	−3.338	12.288	0.9914

temperatures. However, at high temperatures (T > 500 °C) this trend is reversed. In other words, the B values became smaller. To explain this behavior, it should be mentioned that recently it was proved that the alkaline external shell produced during the CO_2 chemisorption may present some microstructural characteristics. Specifically, Martinez-dlCruz and Pfeiffer[46] showed that the Na_2CO_3−ZrO_2 external shell, produced during the CO_2 capture on Na_2ZrO_3, is mesoporous when it is produced at low temperatures. Therefore, under these thermal conditions the CO_2 chemisorption process was not limited to the bulk diffusion processes. To analyze if the $Li_{4+x}(Si_{1-x}Al_x)O_4$ solid solutions present a similar behavior, which would explain the A and B pre-exponential values, some of the CO_2 chemisorption products were analyzed by N_2 adsorption. Table 4 shows the surface area and porous characteristics

Table 4. Microstructural Features of $Li_{4+x}(Si_{1-x}Al_x)O_4$ after CO_2 Chemisorption at 450 and 500°C

sample	S ($_{BET}$ m^2/g)	r_{porous} (nm)
	450 °C	
10m	5.3397	1.88
30m	4.9853	1.88
50m	8.6616	1.88
	500 °C	
10m	3.2626	1.88
30m	4.02836	1.963
50m	4.46063	1.963

measured on the different samples after the CO_2 chemisorption test at 450 and 500 °C, which correspond to the temperatures where the A and B values tended to be reversed. As it can be seen, all the samples presented higher surface areas than fresh samples, and the surface area decreased as a function of the aluminum content. The results are in agreement with the surface area values observed on the original samples (Table 1), and the same results strongly suggest the presence of some mesopores in the samples which might explain the differences observed in the pre-exponential values.

To analyze quantitatively the temperature and aluminum content dependence of the different processes, the Eyring's model was used (eq 4), as it can be used on solid−gas systems

$$\ln(k_i/T) = -(\Delta H^{\ddagger}/RT) + \ln E + \Delta S^{\ddagger}/R \quad (4)$$

where k_i is the rate constant value of the process i; E represents a pre-exponential factor, which in Eyring's formulation is equal to the ratio of Boltzmann's constant to Planck's constant; R is the ideal gas constant; and $\Delta H^{\ddagger}$ and $\Delta S^{\ddagger}$ are the activation enthalpy and entropy, respectively.

Although both constant values were fitted to Eyring's model, only the CO_2 direct chemisorption (k_1) presented a linear behavior, as in the k_2 case the values obtained did not present any specific trend. Perhaps, in the second case, the presence of several diffusion processes does not allow use of this model. In Figure 8, it is clear that all the plots of CO_2 direct chemisorption describe linear trends, fitting Eyring's model.

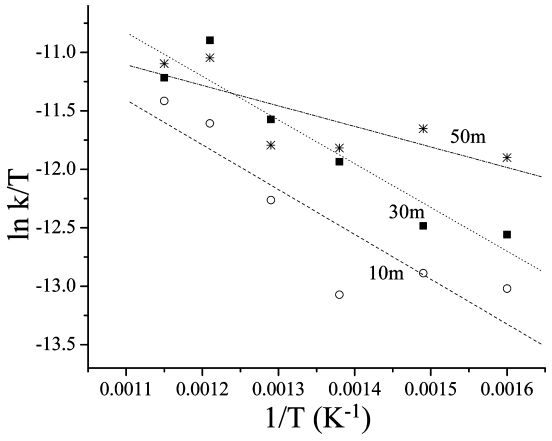

Figure 8. Eyring's plots for the k_1 constant values (CO_2 direct chemisorption) for the different $Li_{4+x}(Si_{1-x}Al_x)O_4$ solid solutions.

dx.doi.org/10.1021/jp4006982 | J. Phys. Chem. C 2013, 117, 6303−6311

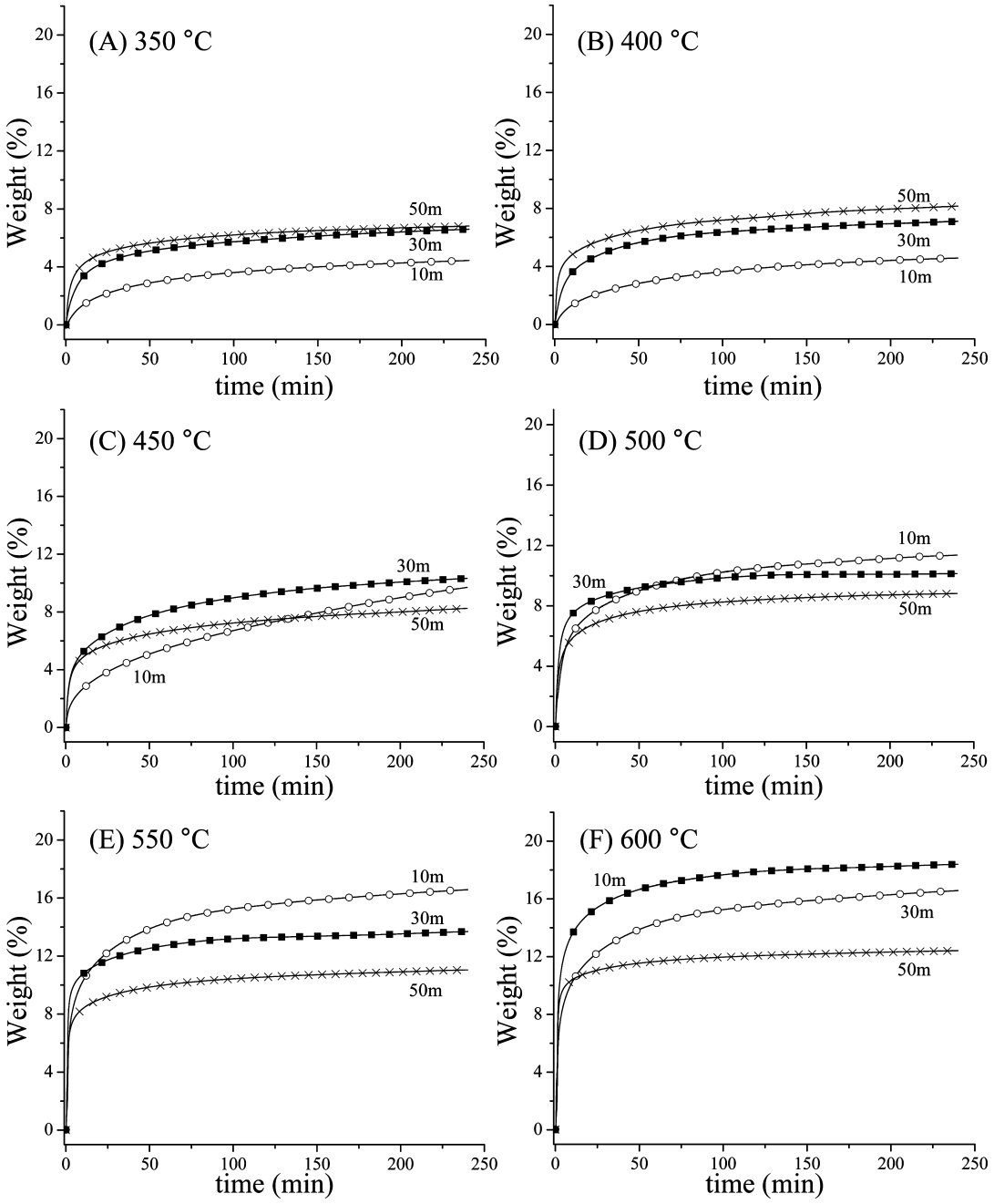

Figure 9. CO_2 capture analyses as a function of the aluminum content, at different temperatures (350−600 °C). The equilibrium process was not reached by any of these curves.

Thus, the $\Delta H^{\ddagger}$ determined were equal to 31.8, 31.1, and 14.6 kJ/mol for 10m, 30m, and 50m, respectively. These results clearly showed that CO_2 direct chemisorption becomes less dependent on temperature as a function of the aluminum content.

To further understand the CO_2 chemisorption produced on the different $Li_{4+x}(Si_{1-x}Al_x)O_4$ solid solutions the curves, previously analyzed, were compared as a function of the aluminum content at the different temperatures. These comparisons are shown in Figure 9. At 350 and 400 °C the CO_2 chemisorption increased mainly as a function of the aluminum content, exhibiting negligible variations as a function of temperature. While the 10m sample chemisorbed ~4.5 wt % after 240 min, the 50m samples increased their weight in 6.8 and 8.2 wt % at 350 and 400 °C, respectively. However, at 450 °C the tendency began to be inversed. At this temperature, while 10m and 30m samples increased their weights at around 9.7 wt % and 10.3 wt %, respectively, the 50m samples chemisorbed less CO_2, 8.0 wt %. In fact, this change in the CO_2 chemisorption tendency was corroborated at 500 °C and higher temperatures, wherein the corresponding weight increments decreased clearly as a function of the aluminum content.

All these results are summarized in the Figure 10, where it is evident that all the samples chemisorbed more CO_2 as a function of temperature, but the aluminum content modified the CO_2 chemisorption trends. At low temperatures (350 and 400 °C) the aluminum content increased the CO_2 chemisorption, although the surface area decreased by the

dx.doi.org/10.1021/jp4006982 | J. Phys. Chem. C 2013, 117, 6303−6311

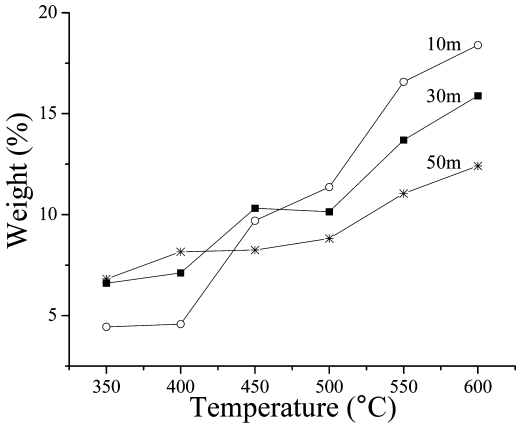

Figure 10. Comparison of the maximum CO_2 capture trends in the different $Li_{4+x}(Si_{1-x}Al_x)O_4$ solid solutions.

aluminum content. In this temperature range the main process is the CO_2 direct chemisorption, which is enhanced by two factors: (1) the increment of basic properties produced over the ceramic particles due to the aluminum addition and therefore due to a lithium excess presence and (2) in this temperature range the Li_2CO_3–Li_2SiO_3–$LiAlO_2$ external shell seems to present some porosity, which allows the CO_2 diffusion and consequently a higher chemisorption. However, at $T \geq 450$ °C the CO_2 chemisorption tends to decrease as a function of the aluminum content, although the total CO_2 chemisorption increased as a function of temperature. This behavior can be explained by the loss of the porosity in the Li_2CO_3–Li_2SiO_3–$LiAlO_2$ external shell due to sintering.[46] As the direct CO_2 chemisorption is limited, the lithium diffusion must be activated and controlled by the different lithium secondary phases present in the external shell. Additionally, whenever aluminum is present in the samples, $LiAlO_2$ is produced as the secondary phase, which only increments the lithium diffusion at temperatures higher than 600 °C.[11] Therefore, in this temperature range (between 450 and 600 °C), $LiAlO_2$ must act as a lithium diffusion inhibitor, reducing the CO_2 chemisorption.

CONCLUSIONS

Different $Li_{4+x}(Si_{1-x}Al_x)O_4$ solid solutions were obtained by a mechanochemical synthesis, and the CO_2 capture experiments were compared to similar experiments performed on the Li_4SiO_4 sample obtained by solid-state reaction, for comparison purposes. Although the XRD results showed that $Li_{4+x}(Si_{1-x}Al_x)O_4$ solid solutions possess similar structural characteristics, the solid-state NMR results strongly suggested that the aluminum sites presented some distortion after the milling process. Additionally, it was probed that the mechanosynthesis tended to increase the $Li_{4+x}(Si_{1-x}Al_x)O_4$ surface areas. Later, these two factors proved to be very important in the CO_2 capture process.

Then, it was observed that aluminum addition and the new microstructural features produced during the milling process importantly increase the CO_2 capture in the following ways, in comparison to the Li_4SiO_4 and $Li_{4+x}(Si_{1-x}Al_x)O_4$ solid solutions prepared by solid-state reaction: (1) The temperature range of the CO_2 chemisorption was significantly increased, and (2) the efficiency tended to increase. All these results were confirmed and supported by an exhaustive kinetic analysis performed in a wide temperature range in the different $Li_{4+x}(Si_{1-x}Al_x)O_4$ solid solutions. Finally, it was observed that the presence of different textural properties obtained in the Li_2CO_3–Li_2SiO_3–$LiAlO_2$ external shell (see reaction 2) may influence the CO_2 chemisorption at low temperatures.

AUTHOR INFORMATION

Corresponding Author

*Phone: +52 (55) 5622 4627. Fax: +52 (55) 5616 1371. E-mail pfeiffer@iim.unam.mx.

Notes

The authors declare no competing financial interest.

ACKNOWLEDGMENTS

This work was financially supported by the project SENER-CONACYT 150358. Authors thank A. Tejeda, G. González-Mancera, and G. Cedillo for technical help.

REFERENCES

(1) Yun-Hang, H., Ed. Advances in CO_2 Conversion and Utilization. *ACS Symposium Series 1056*; American Chemical Society: Washington DC, 2010.
(2) Choi, S.; Drese, J. H.; Jones, C. W. *ChemSusChem* **2009**, *2*, 796–854.
(3) Busch, A.; Alles, S.; Gensterblum, Y.; Prinz, D.; Dewhurst, D. N.; Raven, M. D.; Stanjek, H.; Krooss, B. M. *Int. J. Greenhouse Gas Control* **2008**, *2*, 297–308.
(4) Nair, B. N.; Burwood, R. P.; Goh, V. J.; Nakagawa, K.; Yamaguchi, T. *Prog. Mater. Sci.* **2009**, *54*, 511–541.
(5) Orr, F. M., Jr. *Energy Environ. Sci.* **2009**, *2*, 449–458.
(6) Mejía-Trejo, V. L.; Fregoso-Israel, E.; Pfeiffer, H. *Chem. Mater.* **2008**, *20*, 7171–7176.
(7) Pfeiffer, H.; Vazquez, C.; Lara, V. H.; Bosch, P. *Chem. Mater.* **2007**, *19*, 922–926.
(8) Pfeiffer, H.; Lima, E.; Bosch, P. *Chem. Mater.* **2006**, *18*, 2642–2647.
(9) Ávalos-Rendón, T. L.; Pfeiffer, H. *Energy Fuels* **2012**, *26*, 3110–3114.
(10) Gauer, C.; Heschel, W. *J. Mater. Sci.* **2006**, *41*, 2405–2409.
(11) Ortiz-Landeros, J.; Ávalos-Rendón, T. L.; Gómez-Yáñez, C.; Pfeiffer, H. *J. Therm. Anal. Calorim.* **2011**, *108*, 647–655.
(12) Olivares-Marín, M.; Castro-Díaz, M.; Drage, T. C.; Maroto-Valer, M. M. *Sep. Purif. Technol.* **2010**, *73*, 415–420.
(13) Pacciani, R.; Torres, J.; Solsona, P.; Coe, C.; Quinn, R.; Hufton, J.; Golden, T.; Vega, L. F. *Environ. Sci. Technol.* **2011**, *45*, 7083–7088.
(14) Olivares-Marín, M.; Drage, T. C.; Maroto-Valer, M. M. *Int. J. Greenhouse Gas Control* **2010**, *4*, 623–629.
(15) Seggiani, M.; Puccini, M.; Vitolo, S. *Int. J. Greenhouse Gas Control* **2011**, *5*, 471–478.
(16) Ávalos-Rendón, T.; Casa-Madrid, J.; Pfeiffer, H. *J. Phys. Chem. A* **2009**, *113*, 6919–6923.
(17) Duan, Y.; Parlinski, K. *Phys. Rev. B* **2011**, *84*, 104113.
(18) Halabi, M. H.; de Croon, M. H. J.; van der Schaaf, J.; Cobden, P. D.; Schouten, J. C. *Chem. Eng. J.* **2011**, *168*, 872–882.
(19) Xiao, Q.; Tang, X.; Liu, Y.; Zhong, Y.; Zhu, W. *Chem. Eng. J.* **2011**, *174*, 231–235.
(20) Iwan, A.; Stephenson, H.; Ketchie, W. C.; Lapkin, A. A. *Chem. Eng. J.* **2009**, *146*, 249–258.
(21) Yin, X. S.; Zhang, Q. H.; Yu, J. G. *Inorg. Chem.* **2011**, *50*, 2844–2850.
(22) Rusten, H. K.; Ochoa-Fernández, E.; Lindborg, H.; Chen, D.; Jakobsen, H. A. *Ind. Eng. Chem. Res.* **2007**, *46*, 8729–8737.
(23) Yin, X. S.; Song, M.; Zhang, Q. H.; Yu, J. G. *Ind. Eng. Chem. Res.* **2010**, *49*, 6593–6598.
(24) Radfarnia, H. R.; Iliuta, M. C. *Ind. Eng. Chem. Res.* **2011**, *50*, 9295–9305.
(25) Yin, X. S.; Li, S. P.; Zhang, Q. H.; Yu, J. G. *J. Am. Ceram. Soc.* **2010**, *93*, 2837–2842.

(26) Xiao, Q.; Liu, Y.; Zhong, Y.; Zhu, W. *J. Mater. Chem.* **2011**, *21*, 3838−3842.
(27) Duan, Y. *J. Renewable Sustainable Energy* **2011**, *3*, 013102.
(28) Wang, K.; Guo, X.; Zhao, P.; Wang, F.; Zheng, C. *J. Hazard. Mater.* **2011**, *189*, 301−307.
(29) Mosqueda, H. A.; Vazquez, C.; Bosch, P.; Pfeiffer, H. *Chem. Mater.* **2006**, *18*, 2307−2310.
(30) Rodríguez-Mosqueda, R.; Pfeiffer, H. *J. Phys. Chem. A* **2010**, *114*, 4535−4541.
(31) Ortiz-Landeros, J.; Gómez-Yáñez, C.; Palacios-Romero, L. M.; Lima, E.; Pfeiffer, H. *J. Phys. Chem. A* **2012**, *116*, 3163−3171.
(32) Quinn, R.; Kitzhoffer, R. J.; Hufton, J. R.; Golden, T. C. *Ind. Eng. Chem. Res.* **2012**, *51*, 9320−9327.
(33) Xiao, Q.; Tang, X.; Zhong, Y.; Zhu, W. *J. Am. Ceram. Soc.* **2012**, *95*, 1544−1548.
(34) Radfarnia, H. R.; Iliuta, M. C. *Separ. Purif. Tech.* **2012**, *93*, 98−106.
(35) Robertson, A. D.; West, A. R.; Ritchie, A. G. *Solid State Ionics* **1997**, *104*, 1−11.
(36) Huggins, R. A. *Electrochim. Acta* **1977**, *22*, 773−781.
(37) Yang, A.; Wang, H.; Li, W.; Shi, J. *J. Am. Ceram. Soc.* **2012**, *95*, 1818−1822.
(38) Ni, J.; Kawabe, Y.; Morishita, M.; Watada, M.; Sakai, T. *J. Power Sources* **2011**, *196*, 8104−8109.
(39) Romero-Ibarra, I. C.; Ortiz-Landeros, J.; Pfeiffer, H. *Thermochim. Acta* **2013**, DOI: org/10.1016/j.tca.2012.11.018.
(40) Lowell, S.; Shields, J. E.; Thomas, M. A. *Characterization of Porous Solids and Powders: Surface Area, Pore Size and Density*; Particle Technology Series; Kluwer Academic Publishers: London, 2004.
(41) McCash, E. M. *Surface Chemistry*; Oxford University Press: Oxford, U.K., 2002.
(42) Qi, Z.; Daying, H.; Yang, l.; Qian, Y.; Zibin, Z. *AIChE* **2013**, *59*, 901−911.
(43) Ochoa-Fernandez, E.; Rusten, H. K.; Jakobsen, H. A.; Rønning, M.; Holmen, A.; Chen, D. *Catal. Today* **2005**, *106*, 41−46.
(44) Lee, D. K.; Baek, I. H.; Yoon, W. L. *Chem. Eng. Sci.* **2004**, *59*, 931−942.
(45) Rusten, H. K.; Ochoa-Fernandez, E.; Lindborg, H.; Chen, D.; Jakobsen, H. A. *Ind. Eng. Chem. Res.* **2007**, *46*, 8729−8737.
(46) Martínez-dlCruz, L.; Pfeiffer, H. *J. Phys. Chem. C* **2012**, *116*, 9675−9680.